

This is the accepted manuscript made available via CHORUS. The article has been published as:

Carrier confinement and bond softening in photoexcited bismuth films

Taeho Shin, Johanna W. Wolfson, Samuel W. Teitelbaum, Maria Kandyla, and Keith A. Nelson

Phys. Rev. B **92**, 184302 — Published 10 November 2015

DOI: [10.1103/PhysRevB.92.184302](https://doi.org/10.1103/PhysRevB.92.184302)

Quantum confinement and bond softening in photoexcited bismuth films

Taeho Shin,^{1,2} Johanna W. Wolfson,¹ Samuel W. Teitelbaum¹, Maria Kandyla,^{1,3}, and Keith A. Nelson^{1*}

¹*Department of Chemistry, Massachusetts Institute of Technology,
Cambridge, MA 02139-4307, USA*

²*Present address: Analytical Science Group, Samsung Advanced Institute of Technology,
Suwon 443-803, Republic of Korea*

³*Present address: Theoretical and Physical Chemistry Institute, National Hellenic
Research Foundation, Athens 116-35, Greece*

**Corresponding author*

**Keith A. Nelson: kanelson@mit.edu*

Abstract

Femtosecond pump-probe spectroscopy of bismuth thin films has revealed strong dependences of reflectivity and phonon frequency on film thickness in the range of 25-40 nm. The reflectivity variations are ascribed to distinct electronic structures originating from the large Fermi wavelength and quantum confinement. The phonon frequency is red-shifted by an amount that increases with decreasing film thickness under the same excitation fluence, indicating carrier density-dependent bond softening that increases due to suppressed diffusion of carriers away from the photoexcited region in thin films. The results have significant implications for nonthermal melting of bismuth as well as lattice heating due to inelastic electron-phonon scattering.

Ultrafast transient reflectivity measurements of many materials have revealed a great deal about photoexcited electrons and phonons including their relaxation dynamics and mechanisms [1–3], their coupling, and their roles in photoinduced processes including phase transitions [4,5]. A prototype sample has been crystalline bismuth [4–20], which shows strong oscillations in time-resolved reflectivity due to coherent oscillations of the A_{1g} optical phonon mode that are initiated upon excitation with a femtosecond laser pulse [9]. Measurements in bismuth motivated the development of the displacive excitation of coherent phonons (DECP) model of the lattice response to ultrafast optical absorption, in which sudden excitation of electrons from the valence to the conduction band leads to a nearly instantaneous alteration of the lattice potential energy surface. Hase *et al.* discovered that the frequency of the A_{1g} mode in bismuth is red-shifted with increasing excitation fluence and is chirped, gradually increasing in frequency with time following excitation [12]. Murray and coworkers showed that the phonon frequency reduction is due to carrier density-dependent softening of the lattice potential, and that photocarrier relaxation dynamics are responsible for the vibrational frequency chirp [13]. More recently, Fritz *et al.* conducted DFT calculations of the lattice potential whose results were consistent with bond softening as a function of carrier density [16]. The calculations further showed that increasing carrier density reduces the Peierls distortion continuously and removes the distortion completely at about 2.7% excitation of the valence electrons, indicating that bismuth may undergo a photoinduced structural phase transition to a higher symmetry phase. The experimental and theoretical results reveal that the lattice structure and interatomic forces are influenced heavily by the carrier density which varies in space and time due to the short (15-nm) optical penetration depth into the sample and the dynamics of carrier diffusion and recombination.

In this Letter, we investigate the effect of carrier diffusion and spatial distribution on ultrafast bond softening in highly photoexcited bismuth. To this end, we performed transient reflectivity experiments on bulk and thin-film bismuth samples. The results show distinct changes in both the transient reflectivity sign and magnitude and in the coherent phonon frequency as a

function of film thickness, indicating strong effects of thickness on both electronic structure and photoexcited carrier spatial distribution and density.

The experiments were conducted in a pump-probe geometry using a 1 kHz repetition rate Ti:sapphire laser system which produces 70 fs pulses centered at $\lambda = 800$ nm. The pump pulse was chopped at 500 Hz, and the pump-induced reflectivity changes of bismuth samples were measured using 800 nm probe pulses and a lock-in amplifier. We also carried out pump-probe experiments using 800 nm pump and variable probe wavelengths that were varied from 560 nm to 880 nm. A portion of the 800 nm pulse was focused into a sapphire crystal to generate a white-light continuum and a 10 nm bandpass filter was used to select the probe wavelength. Both pump and probe pulses were p-polarized. A (111)-oriented bulk single crystal and four polycrystalline thin films with different thickness values were used. The films were prepared on silica glass or silicon substrates by sputtering deposition. X-ray crystallographic measurements show that they are all polycrystalline and no distinct structural differences were observed. The thicknesses of the films were determined by ellipsometry.

Figure 1 shows the time-resolved reflectivity of photoexcited bismuth as a function of film thickness. All the traces show gradually varying reflectivity changes due to the photoexcited carriers and time-dependent oscillations due to the A_{1g} coherent phonons launched via DECP. However, several clear differences are observed in the data from different samples.

----- figure 1-----

First, the electronic signal shows a strong thickness dependence. For the bulk sample and a 300 nm film, the signal increases to a positive value upon photoexcitation and then decays gradually as has been reported previously [10,14,18,19]. Despite the large thickness of 300 nm compared to the optical penetration depth (~ 15 nm), a slightly different behavior is observed between the bulk and 300 nm film. This is due mainly to structural differences, because the bulk sample is a single crystal polished along the (111) face, while the film is polycrystalline. In contrast to the bulk and 300-nm thick film, the photoinduced change in reflectivity is negative in

sign for thinner films. The spectral change implies variations in the intrinsic electronic structure of bismuth films as a function of thickness in the 25-40 nm range. Since the Fermi wavelength is ~ 40 nm in bismuth (as opposed to sub-nm in most metals [21]), quantum confinement occurs in films of this dimension or thinner. It has been reported that due to quantum confinement, bismuth is a semiconductor at dimensions below about 30 nm [22–26].

To further investigate the electronic structures of the thin films, we measured the transient reflectivity as a function of probe wavelength from 600 to 880 nm and over a temporal range that was extended to 70 ps. In the case of bulk bismuth as presented in Figs. 2(a) and (b), for long wavelengths from 700 to 850 nm, the background reflectivity increases initially near the time origin and then decays to its minimum around 25–30 ps. For short wavelengths from 600 to 640 nm, the reflectivity decreases to a negative value at the time origin and continues to decrease until 25–30 ps. In contrast to bulk bismuth, the photoinduced reflectivity change of a 25-nm thin film on silica glass is always negative regardless of the probe wavelength as shown in Figs. 3(a) and (b). The magnitude of the change is largest near 640 nm, as it is in the bulk sample. In thin films, an acoustic phonon pulse is observed around 20 ps, and a secondary reflection at 40 ps. Strong oscillations in reflectivity from the A_{1g} phonon mode appear for all probe wavelengths in all the samples, but the thin films show a smaller oscillation amplitude compared to the bulk and 300-nm film (in Figs. 1-3). This is consistent with recent work on Bi_2Te_3 in which oscillations are greatly reduced in very thin films due to a weak gradient force [27].

----- figure 2-----

----- figure 3-----

The transient reflectivity during the first several picoseconds is strongly affected by the photoexcited carrier density as well as the elevated electron temperature. Carriers lose most of their energy to the lattice within ~ 5 ps due to electron-phonon coupling and carriers undergo electron-hole recombination in ~ 15 ps [30]. Accordingly, the transient reflectivity at later times ($> \sim 10$ –20 ps) in Figs. 2 and 3 is described mainly by the elevated electron temperature and the

consequent change in electron population governed by the Fermi-Dirac distribution function [1]. For photon energies near an interband transition, the dominant contribution to the reflectivity change is smearing of the band occupation due to the elevated electron temperature. If we define a Gaussian lineshape $W(E_{ph})$ for the interband transition that is represented phenomenologically by the central transition energy E_{g0} and a linewidth σ , then the corresponding change in electron population due to the electron temperature change from T_0 to T_l is determined by the lineshape $W(E_{ph})$ and the Fermi-Dirac distribution $P(E_{ph}, T)$ as follows:

$$\Delta P(E_{ph}) = \int_0^\infty W(E_{g,i}) [P(E_{ph}, T_1) - P(E_{ph}, T_0)] dE_{gi}, \quad (1)$$

where

$$W(E_{ph}) = \exp \left[-\frac{(E_g - E_{g0})^2}{2\sigma^2} \right], \quad (2)$$

$$P(E_{ph}, T) = \frac{1}{1 + \exp(E_{ph} - E_g)/kT)}. \quad (3)$$

Equation 1 was fit to the wavelength-dependent transient reflectivity at 10 ps delay time of thin films shown in Figs. 2 and 3 (normalized by the value at peak wavelength) with the transition energy E_{g0} and linewidth σ as adjustable parameters. Fitting results are presented in table 1 and in Fig. 4. Our measurements covered the red side of the reflectivity spectrum, showing the expected decrease in reflectivity due to the shifting of the spectrum toward the blue at elevated electron temperatures. The interband transition energy E_{g0} of the thin films blueshifts by 100-200 meV compared to 300 nm film and bulk bismuth. This is due to size-driven quantum confinement [22-26]. The linewidth σ also increases for the thinner films, possibly due to inhomogeneity or due to intrinsic changes in the electron dispersion relation in which the different bands are not parallel. The transition is associated with the $4 \rightarrow 6$ transition at the L point, in which the final state energy is at or near the Fermi energy E_F [28,29].

-----figure 4-----

Table 1: Variation of the interband transition energy with film thickness

Film thickness	E_{g0} (eV)	σ (eV)
25 nm	2.31	0.35
30 nm	2.36	0.37
38 nm	2.39	0.35
300 nm	2.25	0.24
Bulk	2.17	0.18

Besides the background reflectivity change in Figs. 1-3, the frequency of the A_{1g} mode oscillations also varies with the sample thickness. This becomes apparent at higher pump fluences as shown in Fig. 5. The oscillation frequency decreases with increasing fluence due to carrier density-dependent bond softening in both bulk and 30 nm samples, but the reduction in frequency is greater in the 30 nm film at the same excitation fluences. This indicates greater bond softening in the thin films.

----- figure 5-----

To determine the phonon parameters, we eliminated the slowly varying electronic signal and extracted the oscillatory component by differentiating the transient reflectivity data and fitting the result to the function:

$$\frac{d}{dt} \frac{\Delta R}{R} \cong A \exp(-t/\tau_p) \sin((\omega_0 + \beta t)t + \phi) \quad (4)$$

where ω_0 and β represent the initial phonon frequency and the linear chirp rate, respectively, and τ_p is the dephasing time.

The initial phonon frequencies ω_0 obtained from the fits are shown in Fig. 6(a) as a function of the pump fluence for the four samples. Extrapolations to the low-fluence limit converge to a constant value around 2.93 THz which is consistent with the bismuth A_{1g} phonon frequency measured by Raman spectroscopy [11]. This implies that the ground state lattice

potential along the A_{1g} mode coordinate is unchanged in bismuth at least down to 25 nm thickness. The frequency shows a linear reduction with increasing pump fluence in all the samples. However, the slope is substantially steeper in thinner films. This is a result of fast carrier diffusion into the film, which extends the distribution of energetic carriers well beyond the penetration depth of ~ 16 nm for our excitation wavelength. Confinement of the carriers within the films by an insulating silica substrate or a native oxide layer over a silicon substrate results in a carrier density that is higher for thinner films.

----- figure 6-----

In order to account for the trend in the phonon frequency red-shift as a function of film thickness, we consider one-dimensional diffusive carrier transport from the photoexcited region at the front into the depth of a sample, with the diffusion length equal to the optical penetration depth $\delta = 16$ nm for our excitation wavelength. The diffusion time τ_s is given by $\delta = \sqrt{2D\tau_s}$ where D is the diffusion coefficient. A broad range of diffusion coefficient values has been reported for bismuth, from as much as 100 cm²/s for the ground state at room temperature [31] to far lower values of 2.3–5 cm²/s based on femtosecond X-ray diffraction [6] and carrier mobility measurements [13,21]. The time τ_s ranges from approximately 0.01 ps to 0.6 ps based on these values. The fastest time is shorter than our excitation pulse duration of 70 fs, and even the slowest time indicates carrier diffusion throughout the films and at least a few tens of nanometers into the bulk sample during the first 1-2 ps. Due to the spatial confinement of carriers within the thin films, they will distribute evenly throughout the film thickness L from the initial exponentially decaying density profile on a timescale of $\tau_L = L^2/2D$ after which the average density throughout the film will be approximately

$$\overline{n(L)} = \frac{F(1-R)}{L\delta} [1 - \exp(-\frac{L}{\delta})] \quad (5)$$

where F , δ , and R are the excitation fluence (photons/cm²), penetration depth, and reflectivity, respectively. Under a fluence of 3 mJ/cm², the densities are 1.2×10²¹/cm³ for 25 nm, 1.0×10²¹/cm³

for 30 nm, and $0.8 \times 10^{21}/\text{cm}^3$ for 38 nm films. Thus confinement yields a significantly higher density of photogenerated carriers within the thinner films until the recombination process is complete, resulting in an increased softening of the phonon frequencies in the thinner films as shown in Fig. 6(a). This scenario is supported qualitatively by the dephasing times shown in Fig. 6(b). The dephasing time decreases exponentially with pump fluence for all the samples but it decreases more quickly in the thinner films. As the density of carriers increases, inelastic carrier-phonon scattering takes place more frequently causing faster dephasing of the coherent phonons. Therefore the higher carrier density of the thin films results in the shorter dephasing time, which is consistent with more pronounced bond softening. Bond softening can be driven also by ultrafast lattice heating upon photoexcitation [19] but in our case it originates from a purely electronic effect because it is characterized by the initial frequency before thermalization between hot electrons and lattice occurs. Thermal accumulation due to successive pump pulses can also affect the phonon dynamics. In the current measurements, however, the pump repetition rate of 500 Hz was low enough to allow full dissipation of the heat deposited by each pulse. In Fig. 6, we were not able to collect data above the fluence of $6 \text{ mJ}/\text{cm}^2$ ($4 \text{ mJ}/\text{cm}^2$ for the 25 nm film) because permanent damage by individual pump pulses was observed on the sample surface. The lower damage fluence for the 25 nm film further suggests that lack of diffusion in thin films results in a higher energy density stored in the film upon photoexcitation by a single pump pulse, and accordingly that a thinner film may require a lower excitation fluence for thermal melting to occur.

Lastly, the initial sharp drop of the reflectivity at the time origin as shown in Fig. 1 is another notable thickness-dependent feature. The drop is barely visible in the bulk sample, whereas it clearly increases with decreasing film thickness. Boschetto *et al.* observed the sharp drop in a bulk sample using 35-fs pulses [18] and noticed that the drop was not produced by a longer 50-fs pulse. They attributed the initial drop to coherent displacement of atoms by the polarization force during the pulse. In their model, the material parameters involved in the

negative drop are the zero-order polarizability, interatomic distance, and density. Since these should not change significantly for thin films, their model does not explain the thickness dependence of the drop. Based on the observation that the magnitude of the drop becomes larger with increasing excitation fluence [18], with decreasing pulse duration [18], and with decreasing film thickness, we deduce that the drop is associated with carrier-electric field interactions or carrier-carrier interactions near the photoexcited surface, out of which carriers escape quickly in the bulk but to a lesser extent in thin films. This result and the absence of any significant change in our measured phonon frequencies during the first few oscillation periods both suggest that the lowest reported values for the carrier diffusivity D are unlikely to be accurate.

We have examined the ultrafast dynamics of carriers and phonons in bismuth as a function of film thickness. Femtosecond transient reflectivity measurements have revealed that the electronic signal is strongly influenced by film thickness at the range of 25–40 nm. We attribute the strong dependence to the large Fermi wavelength and to the resulting quantum confinement effect. The red-shift of the A_{1g} phonon frequency is greater in thinner films at the same excitation fluence because a higher density of photogenerated carriers is confined within a thinner film. Carrier density effects appear to be responsible for a strong thickness-dependence in the initial induced reflectivity as well. Our studies have important implications for ultrafast nonthermal melting of bismuth which is believed to occur upon strong photoexcitation [4,32]. The present results imply that a thinner film would undergo the phase transition at lower pump fluence than a bulk sample because of higher carrier density. We also infer that the confined hot carriers result in greater lattice heating in thinner films. Thus both nonthermal and thermal melting are facilitated in thinner films. Quantum confinement and changes in the electronic structure of the samples, from semimetal in bulk and thick layers to semiconductor in thin films, may have additional effects on melting and other photoinduced responses.

This research was supported by grants from the Office of Naval Research (N00014-12-1-0530) and the National Science Foundation (CHE-1111557).

References

- [1] R. Schoenlein, W. Lin, J. Fujimoto, and G. Eesley, Phys. Rev. Lett. **58**, 1680 (1987).
- [2] R.W. Schoenlein, W.Z. Lin, E.P. Ippen, and J.G. Fujimoto, Appl. Phys. Lett. **51**, 1442 (1987).
- [3] S. Wall, D. Prabhakaran, A. Boothroyd, and A. Cavalleri, Phys. Rev. Lett. **103**, 097402 (2009).
- [4] K. Sokolowski-Tinten, C. Blome, J. Blums, A. Cavalleri, C. Dietrich, A. Tarasevitch, I. Uschmann, E. Förster, M. Kammler, M. Horn-von-Hoegen, and D. von der Linde, Nature **422**, 287 (2003).
- [5] M. Chollet, L. Guerin, N. Uchida, S. Fukaya, H. Shimoda, T. Ishikawa, K. Matsuda, T. Hasegawa, A. Ota, H. Yamochi, G. Saito, R. Tazaki, S.-I. Adachi, and S.-Y. Koshihara, Science **307**, 86 (2005).
- [6] S. Johnson, P. Beaud, C. Milne, F. Krasniqi, E. Zijlstra, M. Garcia, M. Kaiser, D. Grolimund, R. Abela, and G. Ingold, Phys. Rev. Lett. **100**, 155501 (2008).
- [7] T. K. Cheng, S. D. Brorson, a. S. Kazeroonian, J. S. Moodera, G. Dresselhaus, M. S. Dresselhaus, and E. P. Ippen, Appl. Phys. Lett. **57**, 1004 (1990).
- [8] T.K. Cheng, J. Vidal, H.J. Zeiger, G. Dresselhaus, M.S. Dresselhaus, and E.P. Ippen, Appl. Phys. Lett. **59**, 1923 (1991).
- [9] H. Zeiger, J. Vidal, T. Cheng, and E. Ippen, Phys. Rev. B **45**, 768 (1992).
- [10] M. DeCamp, D. Reis, P. Bucksbaum, and R. Merlin, Phys. Rev. B **64**, 092301 (2001).
- [11] M. Hase, K. Mizoguchi, H. Harima, S. Nakashima, and K. Sakai, Phys. Rev. B **58**, 5448 (1998).
- [12] M. Hase, M. Kitajima, S. Nakashima, and K. Mizoguchi, Phys. Rev. Lett. **88**, 067401 (2002).
- [13] S. Fahy and D. Reis, Phys. Rev. Lett. **93**, 109701 (2004).
- [14] É. Murray, D. Fritz, J. Wahlstrand, S. Fahy, and D. Reis, Phys. Rev. B **72**, 060301 (2005).
- [15] É. Murray, S. Fahy, D. Prendergast, T. Ogitsu, D. Fritz, and D. Reis, Phys. Rev. B **75**, 184301 (2007).
- [16] D.M. Fritz, D.A. Reis, B. Adams, R.A. Akre, J. Arthur, C. Blome, P.H. Bucksbaum, A.L. Cavalieri, S. Engemann, S. Fahy, R.W. Falcone, P.H. Fuoss, K.J. Gaffney, M.J. George, J. Hajdu, M.P. Hertlein, P.B. Hillyard, M. Horn-von Hoegen, M. Kammler, J. Kaspar, R. Kienberger, P. Krejcik, S.H. Lee, A.M. Lindenberg, B. McFarland, D. Meyer, T.

Montagne, E.D. Murray, A.J. Nelson, M. Nicoul, R. Pahl, J. Rudati, H. Schlarb, D.P. Siddons, K. Sokolowski-Tinten, T. Tschentscher, D. von der Linde, and J.B. Hastings, *Science* **315**, 633 (2007).

- [17] A.Q. Wu and X. Xu, *Appl. Surf. Sci.* **253**, 6301 (2007).
- [18] D. Boschetto, E. Gamaly, A. Rode, B. Luther-Davies, D. Glijer, T. Garl, O. Albert, A. Rousse, and J. Etchepare, *Phys. Rev. Lett.* **100**, 027404 (2008).
- [19] T. Garl, E.G. Gamaly, D. Boschetto, A. V. Rode, B. Luther-Davies, and A. Rousse, *Phys. Rev. B* **78**, 134302 (2008).
- [20] O. Misochko, M. Hase, K. Ishioka, and M. Kitajima, *Phys. Rev. Lett.* **92**, 197401 (2004).
- [21] N. Garcia, Y. Kao, and M. Strongin, *Phys. Rev. B* **5**, 2029 (1972).
- [22] E.I. Rogacheva, S.N. Grigorov, O.N. Nashchekina, S. Lyubchenko, and M.S. Dresselhaus, *Appl. Phys. Lett.* **82**, 2628 (2003).
- [23] V. N. Lutsii, *Sov. Phys. JETP Lett.* **2**, 245 (1965).
- [24] V. Sandomirskii, *Sov. Phys. JETP* **25**, 101 (1967).
- [25] C. Hoffman, J. Meyer, F. Bartoli, and A. Di Venere, *Phys. Rev. B* **48**, 431 (1993).
- [26] E.I. Rogacheva, S.G. Lyubchenko, and M.S. Dresselhaus, *Thin Solid Films* **516**, 3411 (2008).
- [27] Y. Wang, L. Guo, and X. Xu, *Phys. Rev. B* **88**, 064307 (2013)
- [28] P. Wang and A. Jain, *Phys. Rev. B* **2**, 2978 (1970).
- [29] S. Golin, *Phys. Rev.* **166**, 643 (1968).
- [30] Y.M. Sheu, Y.J. Chien, C. Uher, S. Fahy, and D. A. Reis, *Phys. Rev. B* **87**, 075429 (2013).
- [31] G. Saunders and Z. Sumengen, *Proc. R. Soc. Lon. Ser-A.* **8**, 453 (1972).
- [32] G. Sciaini, M. Harb, S.G. Kruglik, T. Payer, C.T. Hebeisen, F.-J.M. zu Heringdorf, M. Yamaguchi, M. Horn-von Hoegen, R. Ernstorfer, and R.J.D. Miller, *Nature* **458**, 56 (2009).

List of Figures

Fig. 1. Transient reflectivity change of bismuth single crystal and thin films at a constant pump fluence of 1 mJ/cm^2 .

Fig. 2. Wavelength-dependent reflectivity of bulk single crystal bismuth with a pump pulse fluence of 6 mJ/cm^2 . (a) Reflectivity change up to 10 ps showing strong coherent phonon oscillations. (b) Dynamics up to 70 ps showing gradual electron cooling.

Fig. 3. Wavelength-dependent reflectivity of a 25 nm bismuth film with a pump pulse fluence of 6 mJ/cm^2 . (a) Reflectivity change up to 5 ps showing strong coherent phonon oscillations. (b) Reflectivity change up to 70 ps showing the acoustic response and gradual electron cooling.

Fig. 4. Fitting results of the wavelength-dependent reflectivity assuming initial (T_0) and final (T_f) temperatures of 293 K and 450 K. Circles represent the transient reflectivity data (normalized) of bismuth samples at 10 ps. The lines represent the fitting to the differential reflectivity given by Eq. 1. The interband transition energy of the thin films blueshifts approximately by 100-200 meV compared to bulk bismuth.

Fig. 5. (a) Transient reflectivity change of bismuth bulk single crystal and (b) of 30 nm thin film on silicon as a function of pump fluence from 0.7 to 6.0 mJ/cm^2 . (c) Comparison of frequency red shift between the bulk and thin film bismuth. More vibrational cycles between two vertical lines are present in the bulk single crystal under a pump fluence of 3.1 mJ/cm^2 . In (a)–(c), the time origin was adjusted to the peak of the first vibrational cycle.

Fig. 6. (a) Initial frequency and (b) the dephasing time of the A_{1g} phonon mode obtained from the

fit.

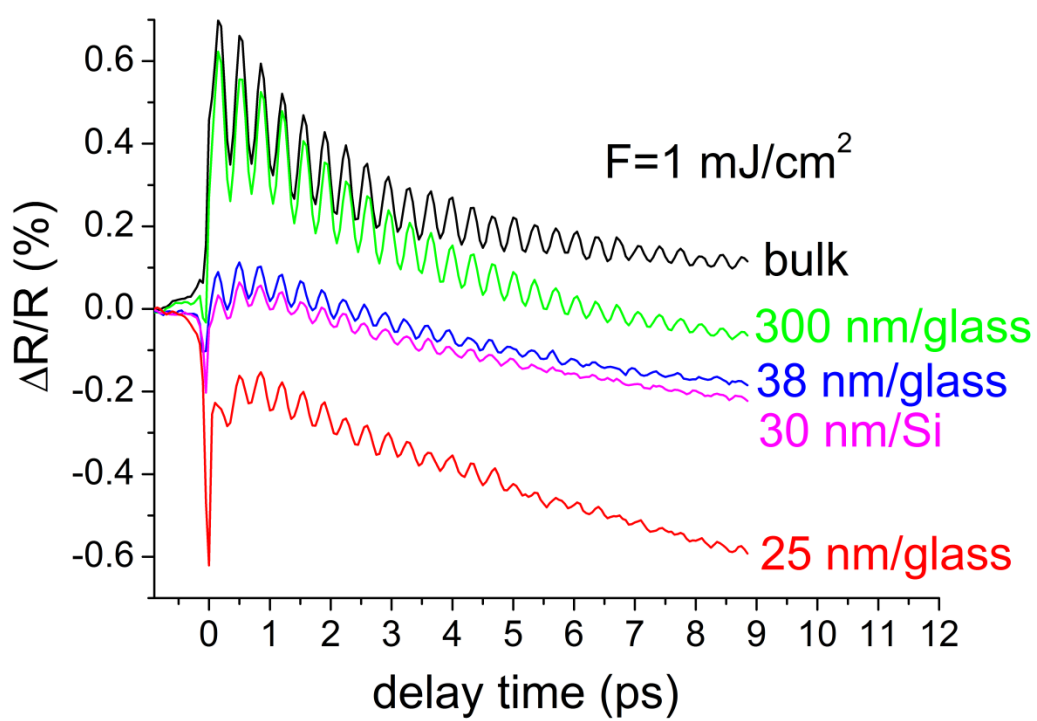


Fig. 1

Shin *et al.*

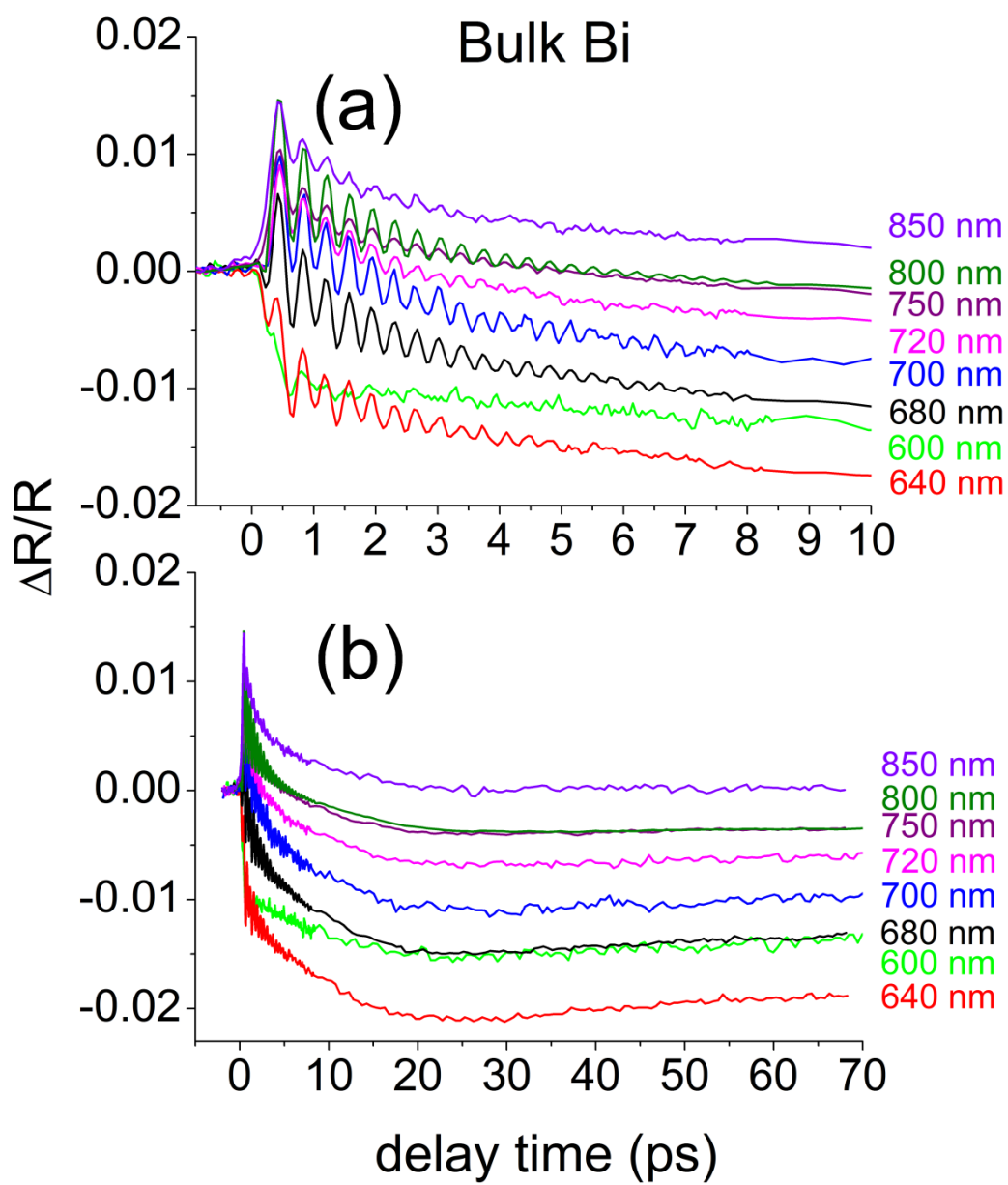


Fig. 2

Shin *et al.*

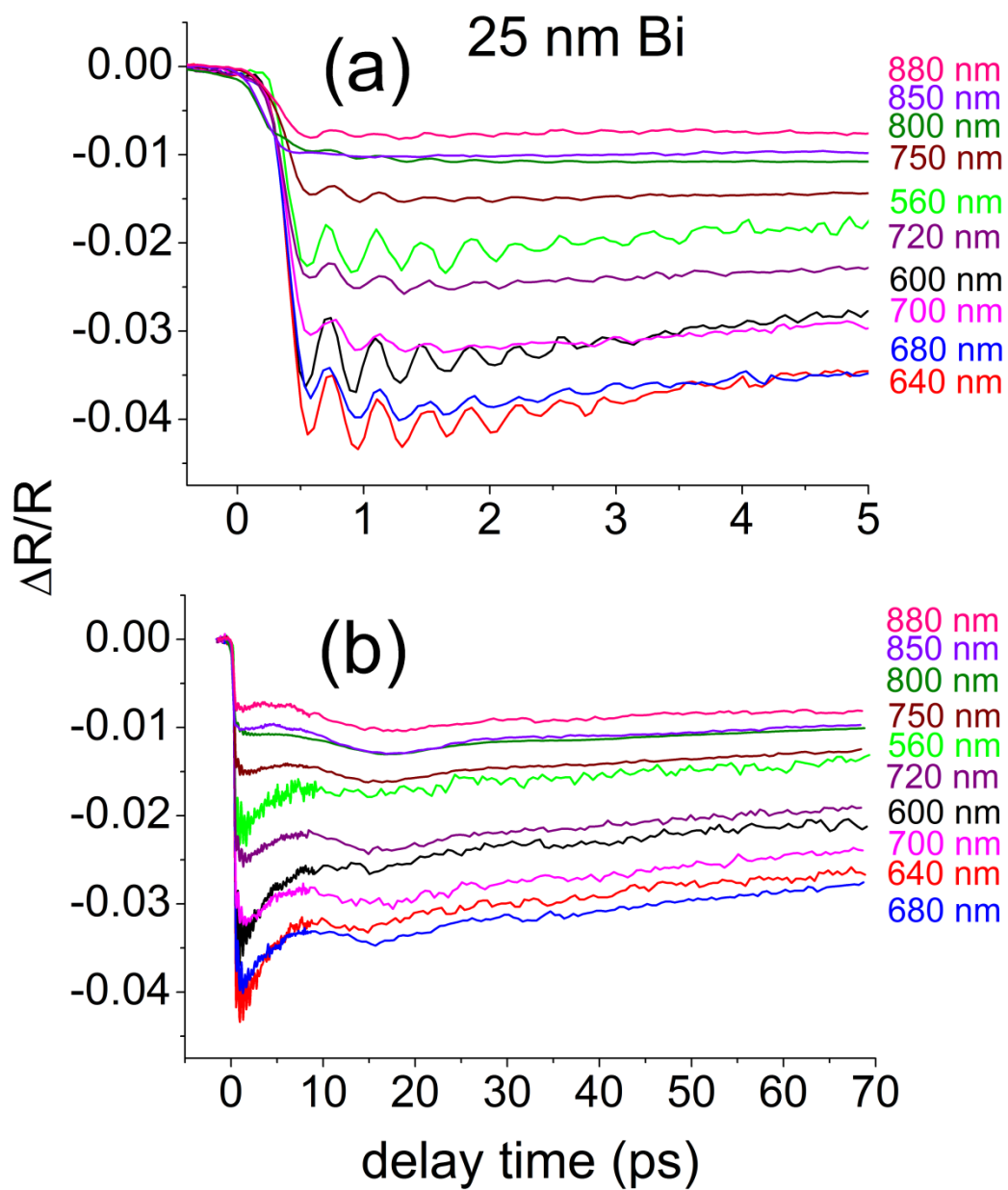


Fig. 3

Shin et al.

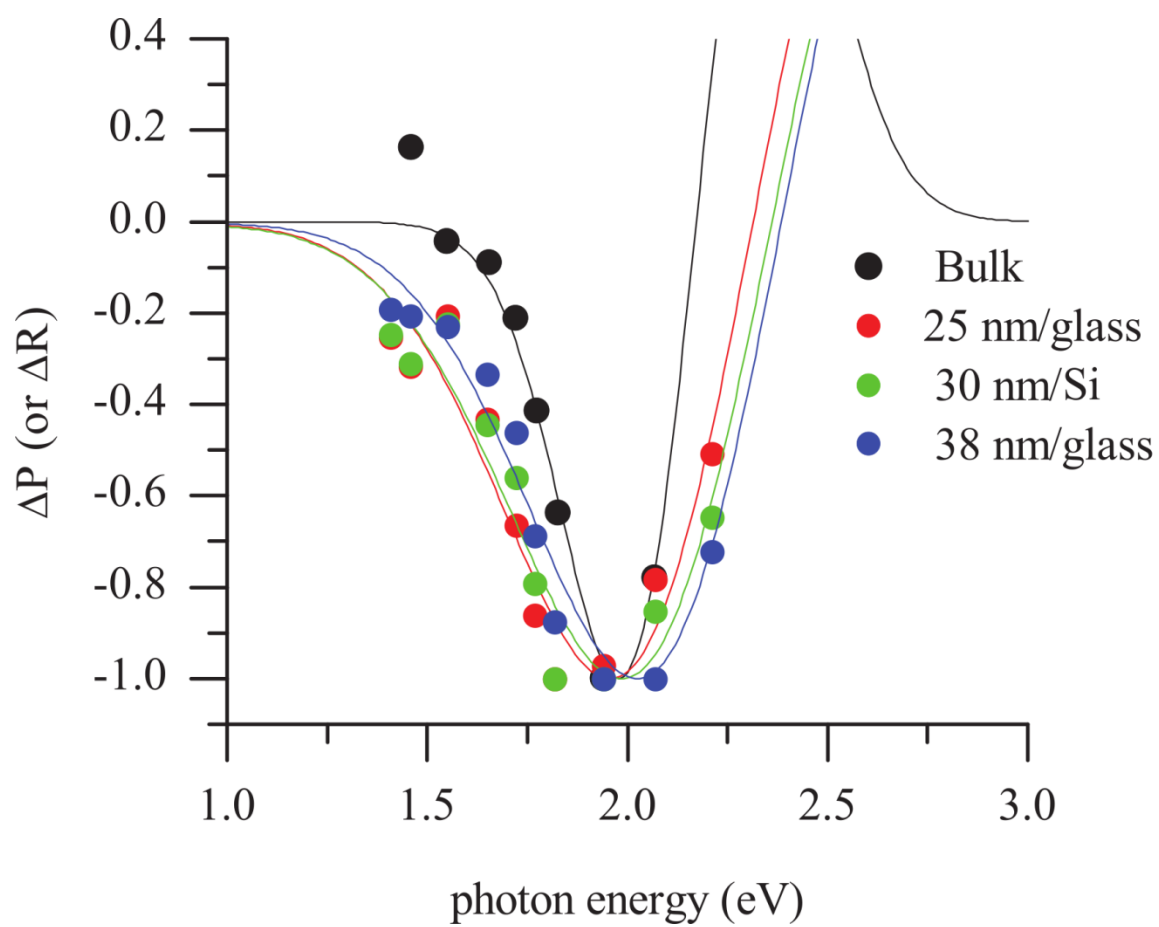


Fig. 4

Shin *et al.*

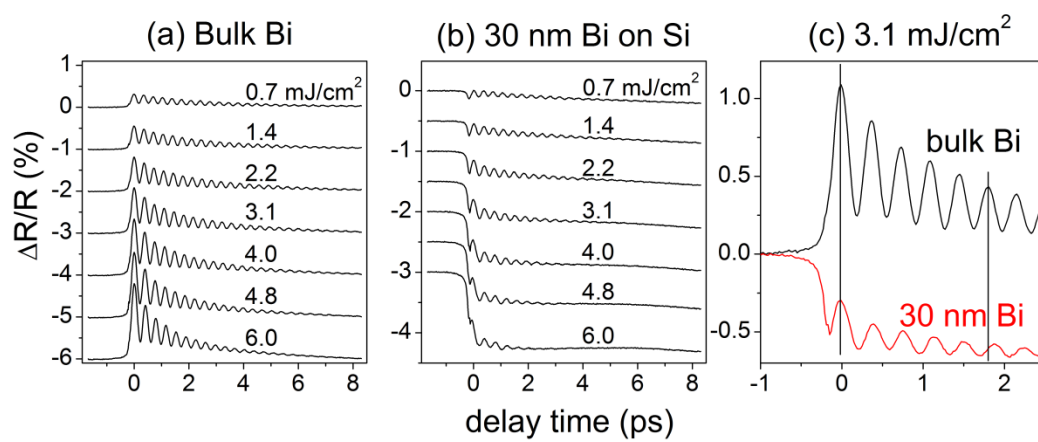


Fig. 5

Shin *et al.*

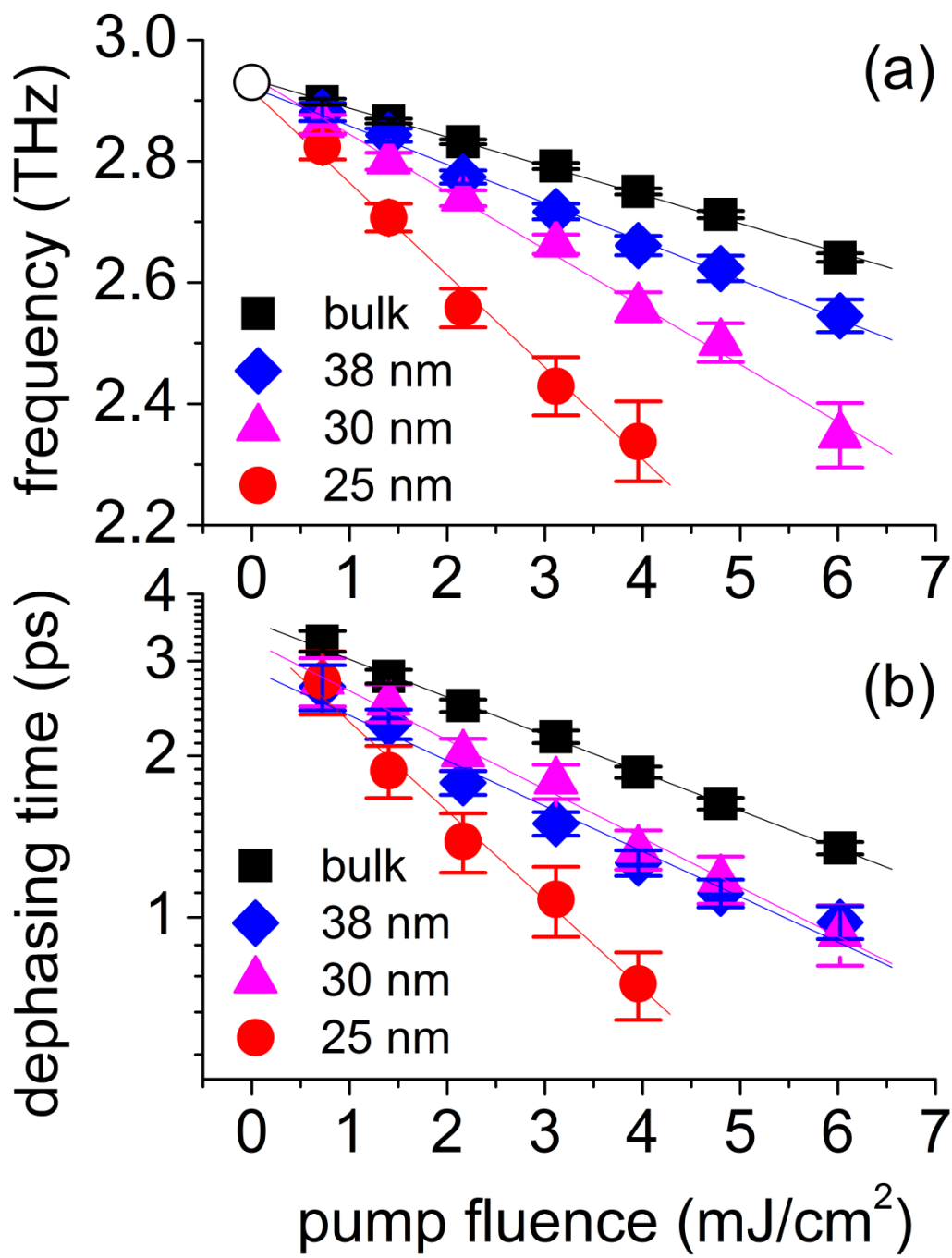


Fig. 6

Shin *et al.*